Sweet Confinement: Glucose and Carbohydrate Osmolytes in Reverse Micelles

Benjamin P. Wiebenga-Sanford, Jack B. Washington, Brett Cosgrove, Eduardo F. Palomares, Derrick A. Vasquez, Christopher D. Rithner, and Nancy E. Levinger*

Department of Chemistry, Colorado State University, Fort Collins, CO 80523

Supporting information

Section S1 includes 2D ROESY NMR methods and a 2D ROESY NMR spectrum of glucose-*loaded* reverse micelles (RMs), 2D NOESY NMR spectra of ethylene glycol, glycerol, meso-erythritol, xylitol, sorbitol and trehalose-*loaded* AOT/isooctane RMs. Section S2 includes additional discussion of potential contributions to apparent RM size reduction, and statistical analysis demonstrating significance of dynamic light scattering results.

S1. 2D NMR Spectra

S1.1 2D ROESY study

To confirm the presence of interactions and interpret the phase of 2D NOESY NMR signals of carbohydrate-*loaded* RMs, we also performed 2D ROESY NMR measurements. ^{1}H-^{1}H-ROESY NMR experiments were performed with a 500 ms mixing time at 25.0 °C using an Inova spectrometer (Varian, Inc., Palo Alto, CA) running VNMRJ software (version 4.2) and operating at 500 MHz for ^{1}H (11.75 T). Spectra are the result of co-adding 32 transients per row with a recovery time of 1.5 s. Chemical shifts, δ, are reported with respect to TMS (0.0 ppm) via substitution from cyclohexane-d_{12}. Acquisition for 2D NMR spectra was performed using the Varian VNMRJ (Linux) software. Phasing and baseline correction of 2D spectra were performed within VNMRJ.

The ROESY spectrum for glucose/water/AOT/isooctane RMs is shown in Fig. S1. The phase of peaks in the ROESY spectrum allows us to identify and assign peaks associated with NOE (phase opposite from diagonal) and those arising from chemical exchange (phase same sign as diagonal).[1]

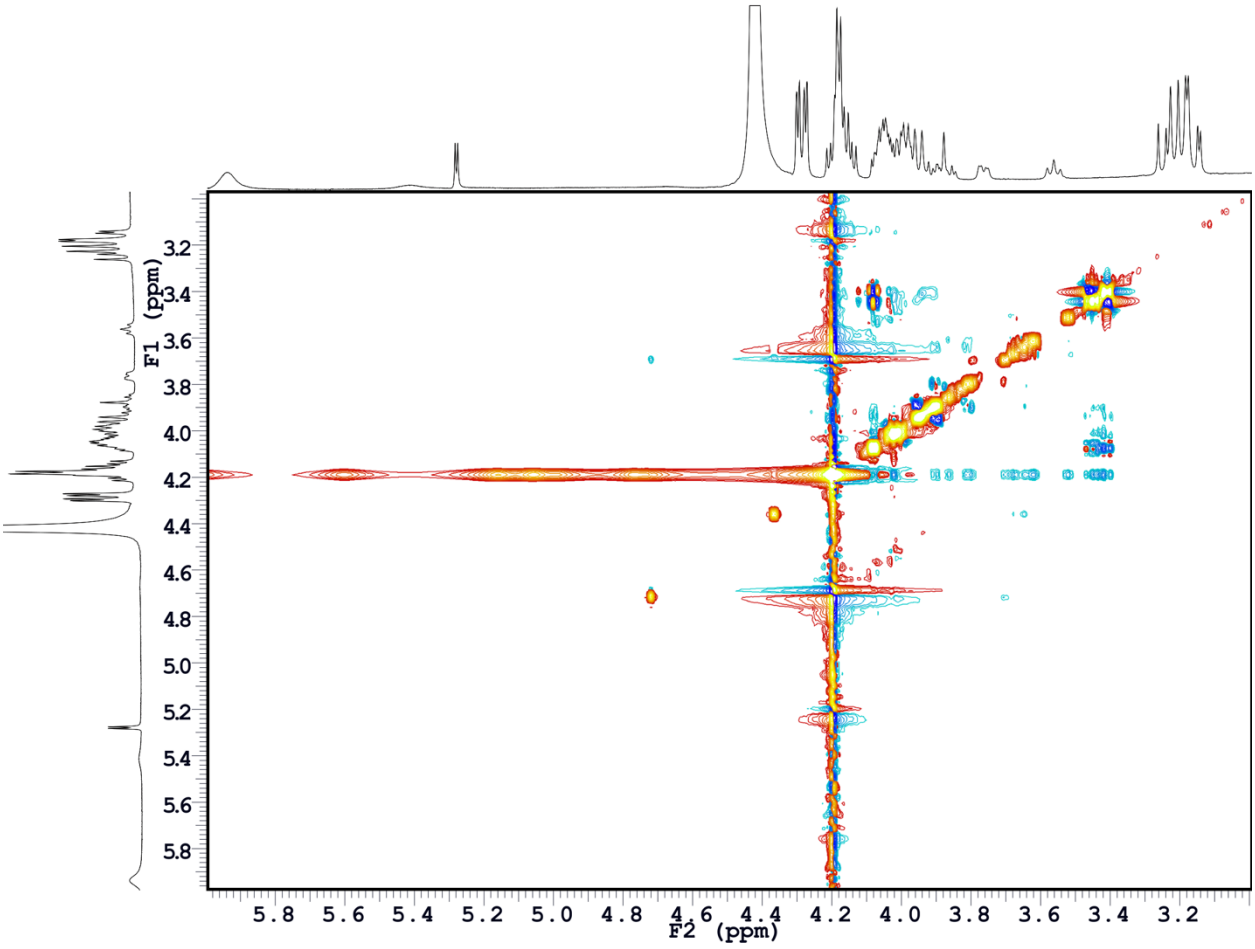

Figure S1. 2D ROESY NMR of w_0=10 glucose-*loaded*/water/2,2,4-trimethylpentane (isooctane). All cross peaks for CH protons display positive phase while cross-peaks between water and glucose OH groups maintain negative phase. This shows that cross peaks with CH protons, including AOT-AOT peaks, arise from NOE interactions while the water-hydroxyl peaks reflect chemical exchange between water and glucose OH groups.

S1.2 2D NOESY NMR of carbohydrates

In addition to our measurements of glucose-*loaded* RMs, we measured 2D NOESY NMR spectra for ethylene glycol, glycerol, meso-erythritol, xylitol, sorbitol, and trehalose-*loaded* AOT RMs. Samples were prepared with the same mass ratio as used for glucose-loaded RMs, for example 90 mg water:30 mg carbohydrate, which is equivalent to a 30 water:1 glucose molecular ratio. ^{1}H-^{1}H-NOESY experiments were performed on a 500 MHz Varian Inova spectrometer and are the result of co-adding 32 transients per row with a recovery time of 1.5 s and mixing time of 200 ms. Chemical shifts, δ, are reported with respect to TMS (0.0 ppm) via substitution from cyclohexane-d_{12} . All experiments were performed at 25.0 °C. Acquisition for 2D NMR spectra was performed using Varian VNMRJ (Linux) software. Phasing and baseline correction of 2D spectra were performed within VNMRJ.

2D NOESY NMR spectra are presented in Figs. S2-S7 below. Notably, we observe the same trends that we see in the glucose containing RMs for all these systems. In addition to the spectra shown, we attempted to measure the 2D NOESY NMR spectrum for myo-inositol in RMs. However, the exceedingly low solubility of myo-inositol in the RM solutions precluded reasonable interpretation of the spectrum.

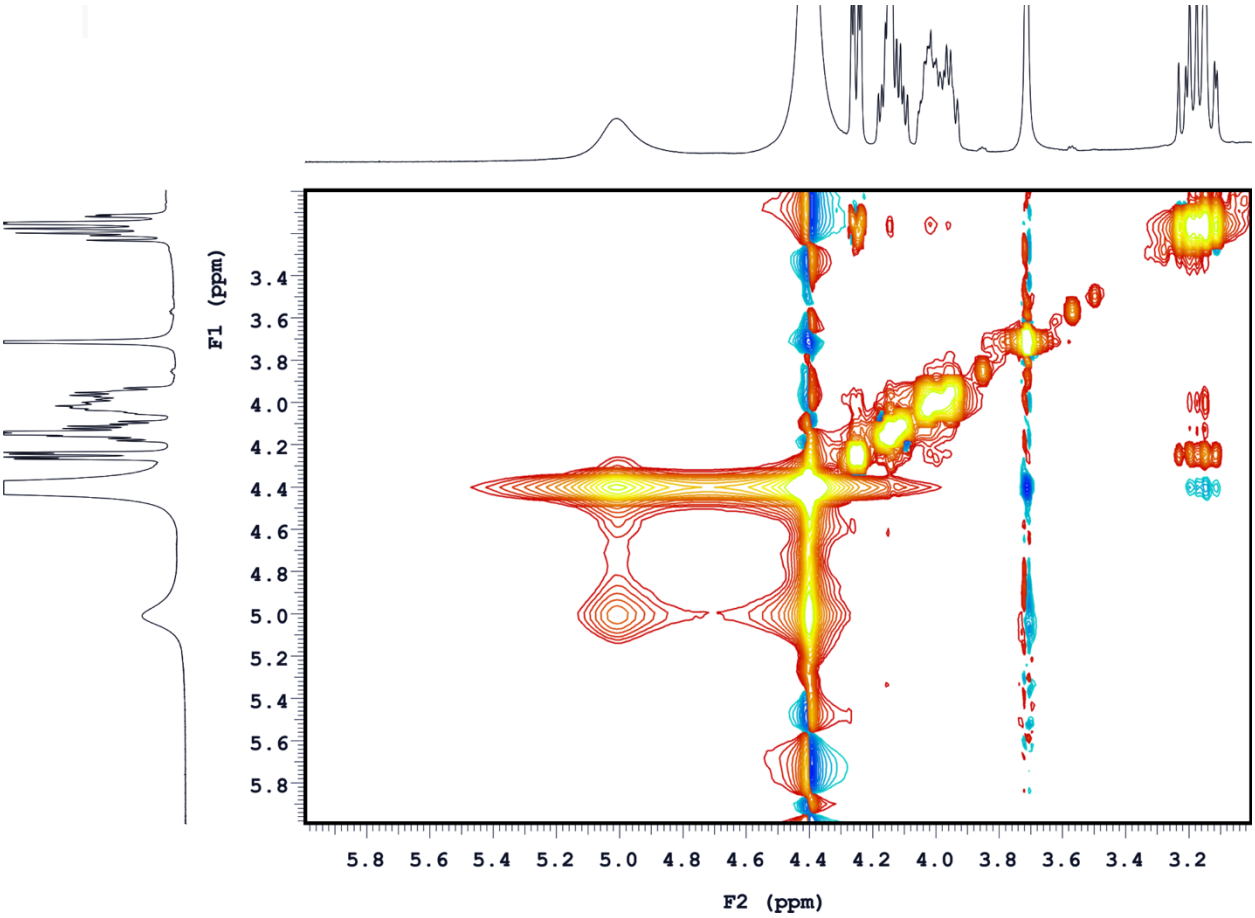

Figure S2. 2D NOESY NMR spectrum of ethylene glycol-*loaded* reverse micelles, w_0=10 ethylene glycol/water/AOT/2,2,4-trimethylpentane reverse micelles. Signals below 3 ppm arise from AOT and 2,2,4-trimethylpentane protons that do not interact with ethylene glycol aliphatic protons. The intense signal at ~4.4 ppm arising from water leads to an artifact in the spectrum. No clear cross-peaks are observed between ethylene glycol and AOT protons.

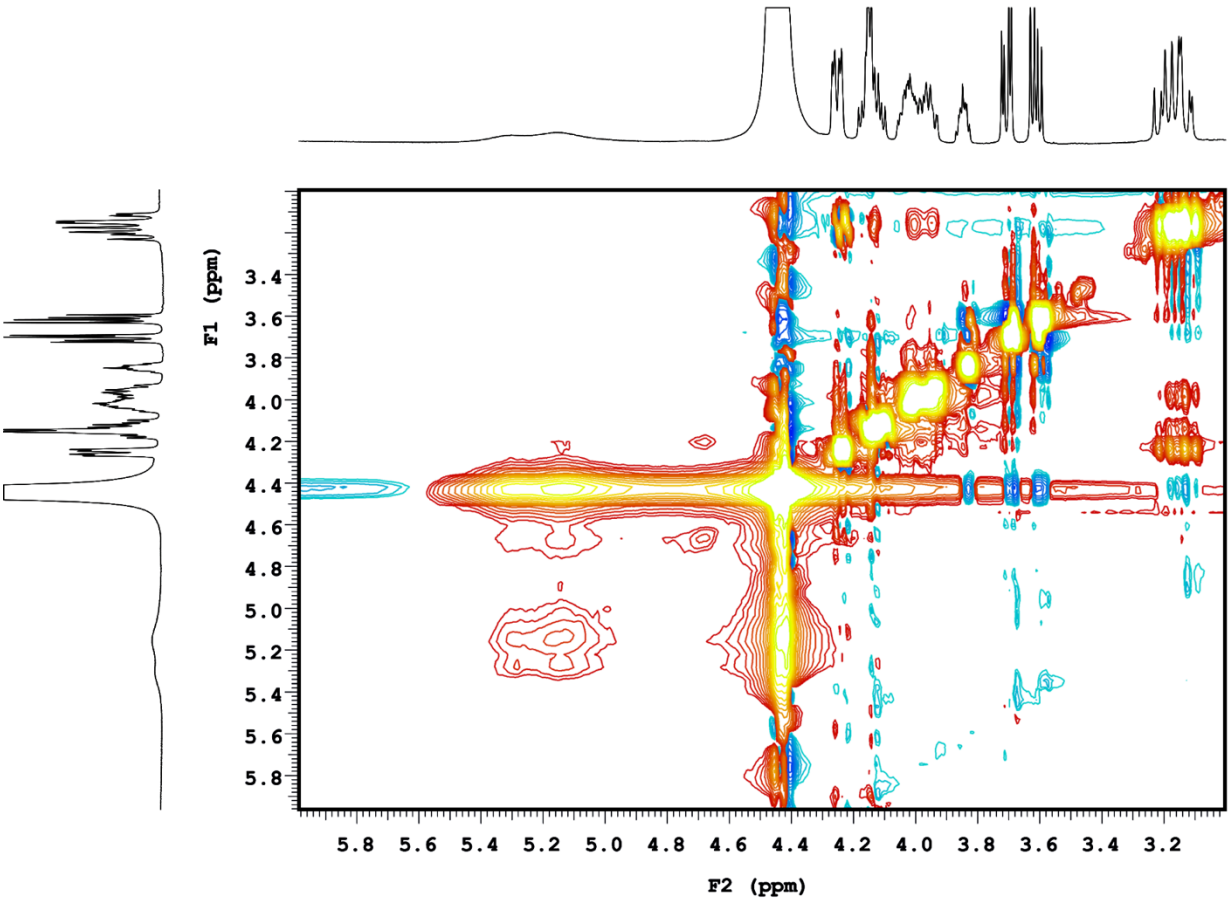

Figure S3. 2D NOESY NMR spectrum of glycerol-*loaded* reverse micelles, w_0=10 glycerol/water/AOT/2,2,4-trimethylpentane reverse micelles. Signals below 3 ppm arise from AOT and 2,2,4-trimethylpentane protons that do not interact with glycerol aliphatic protons. The intense signal at ~4.45 ppm arising from water leads to an artifact in the spectrum. No clear cross-peaks are observed between glycerol and AOT protons.

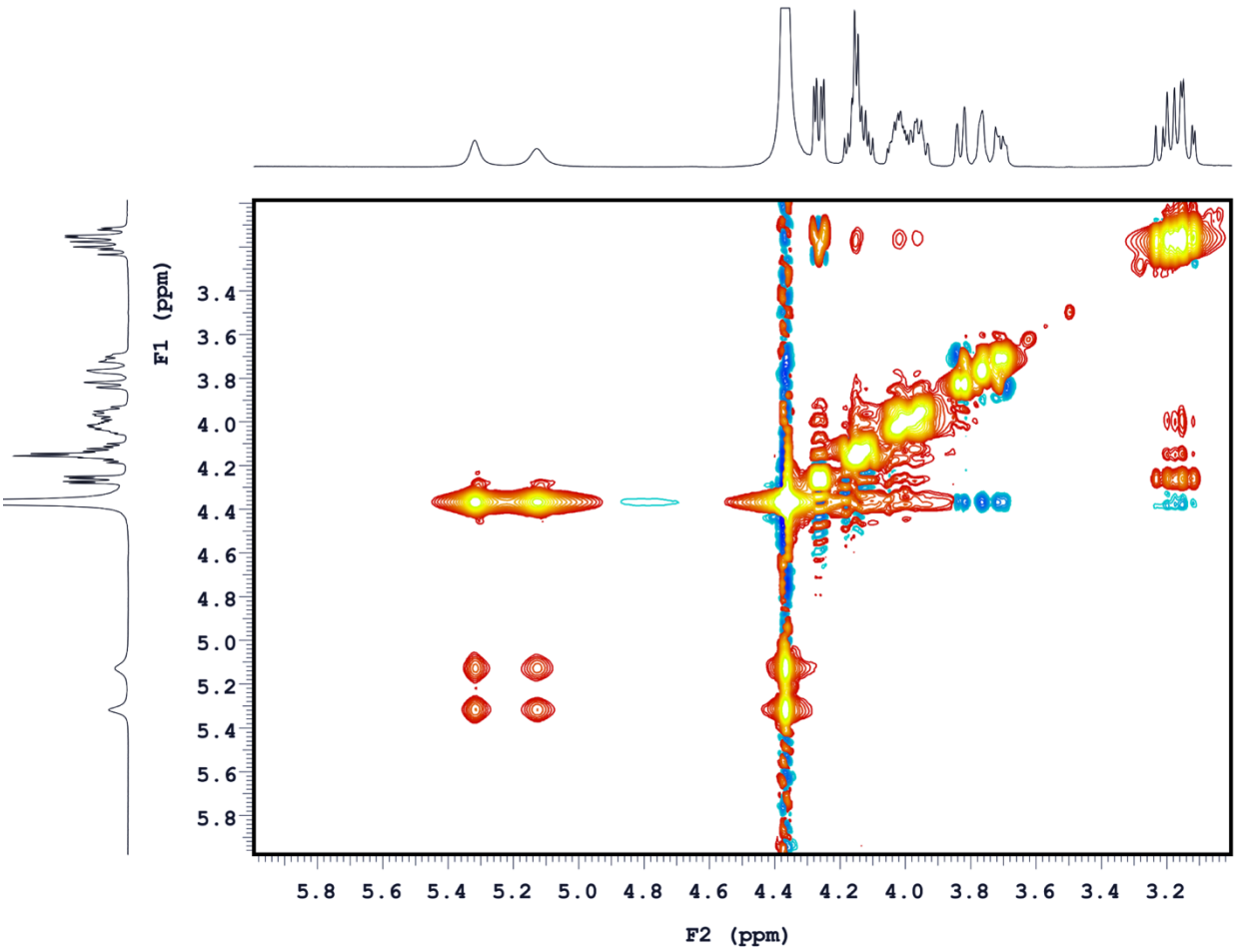

Figure S4. 2D NOESY NMR spectrum of meso-erythritol-*loaded* reverse micelles, w_0=10 erythritol/water/AOT/2,2,4-trimethylpentane reverse micelles. Signals below 3 ppm arise from AOT and 2,2,4-trimethylpentane protons that do not interact with erythritol aliphatic protons. The intense signal at ~4.35 ppm arising from water leads to an artifact in the spectrum. No clear cross-peaks are observed between erythritol and AOT protons.

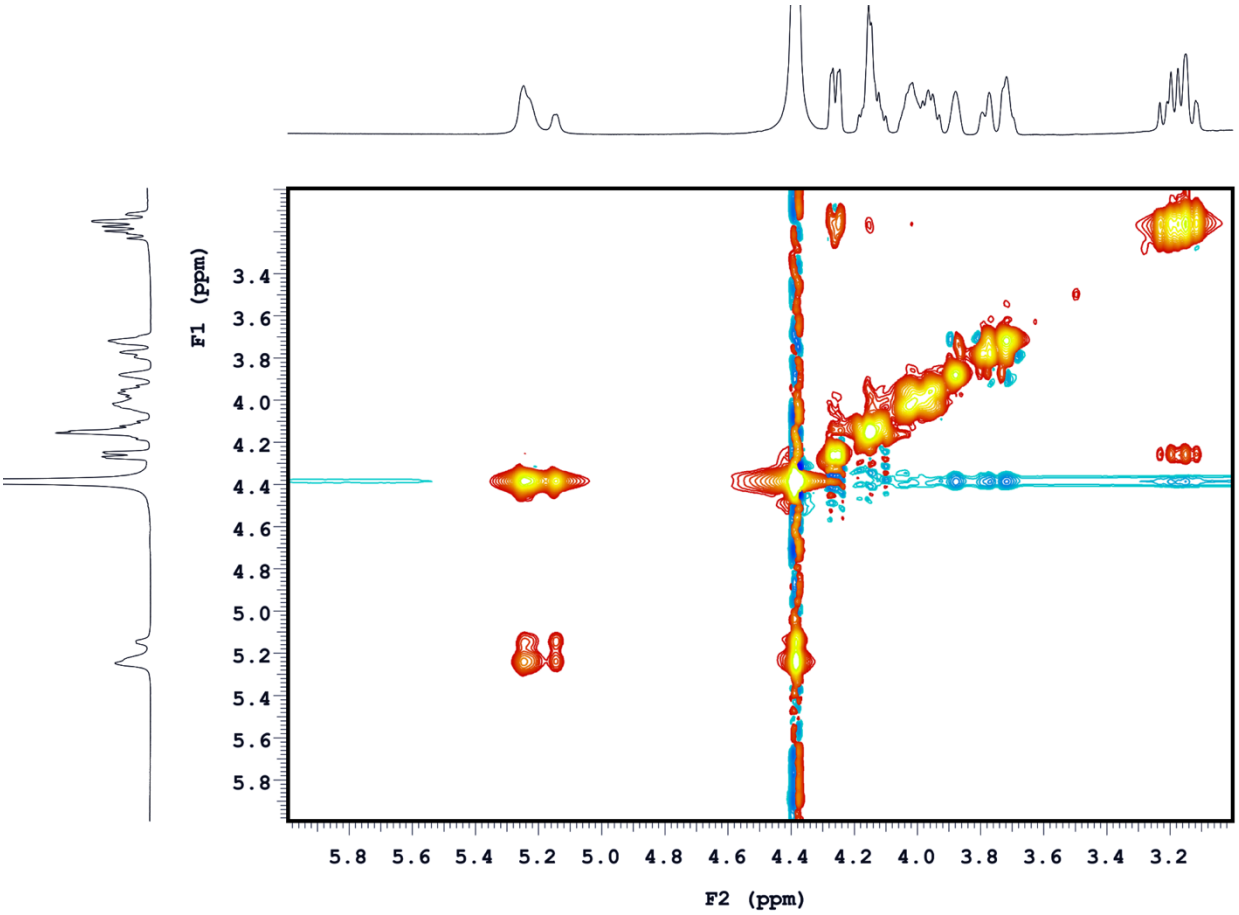

Figure S5. 2D NOESY NMR spectrum of xylitol-*loaded* reverse micelles, w_0=10 xylitol/water/AOT/2,2,4-trimethylpentane reverse micelles. Signals below 3 ppm arise from AOT and 2,2,4-trimethylpentane protons that do not interact with xylitol aliphatic protons. The intense signal at ~4.35 ppm arising from water leads to an artifact in the spectrum. No clear cross-peaks are observed between xylitol and AOT protons.

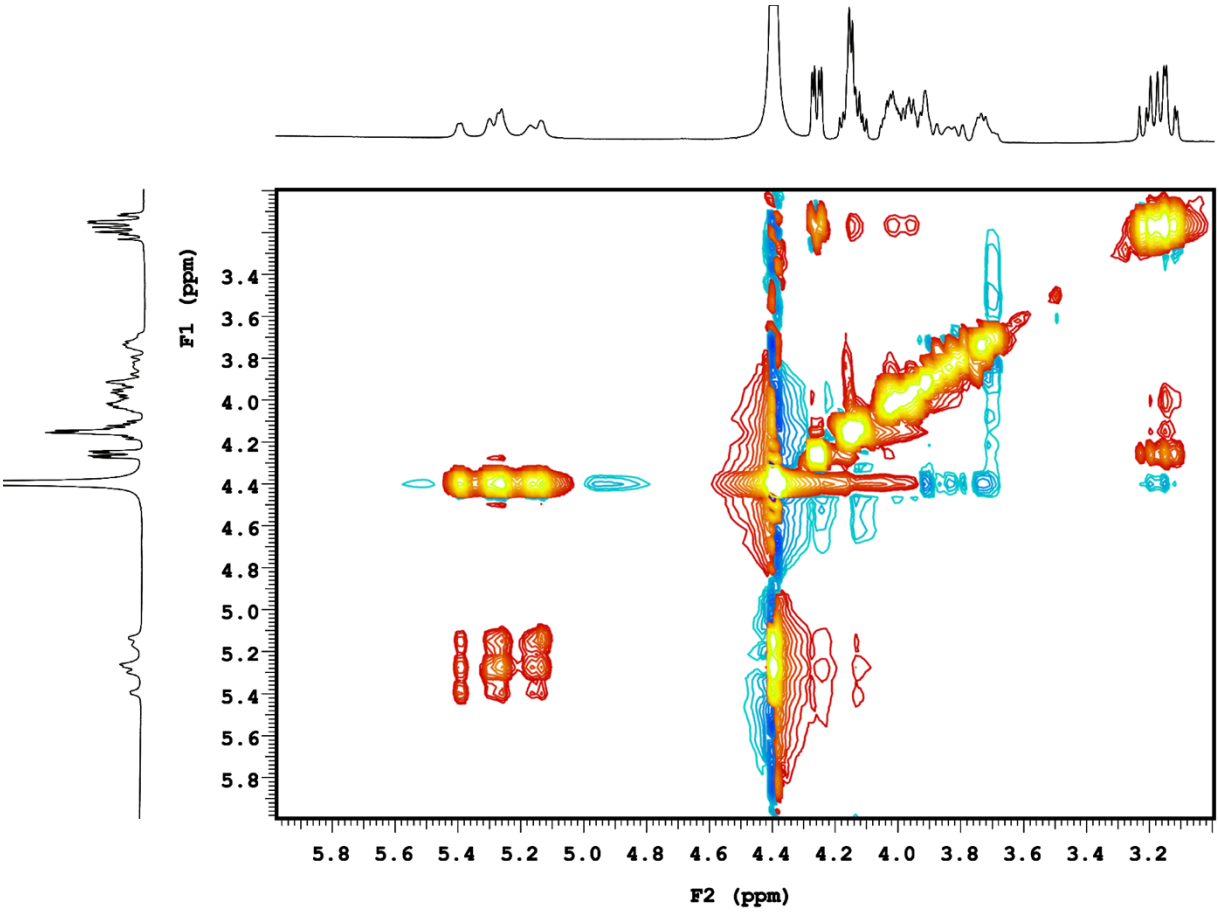

Figure S6. 2D NOESY NMR spectrum of sorbitol-*loaded* reverse micelles, w_0=10 sorbitol/water/AOT/2,2,4-trimethylpentane reverse micelles. Signals below 3 ppm arise from AOT and 2,2,4-trimethylpentane protons that do not interact with sorbitol aliphatic protons. The intense signal at ~4.4 ppm arising from water leads to an artifact in the spectrum. No clear cross-peaks are observed between sorbitol and AOT protons.

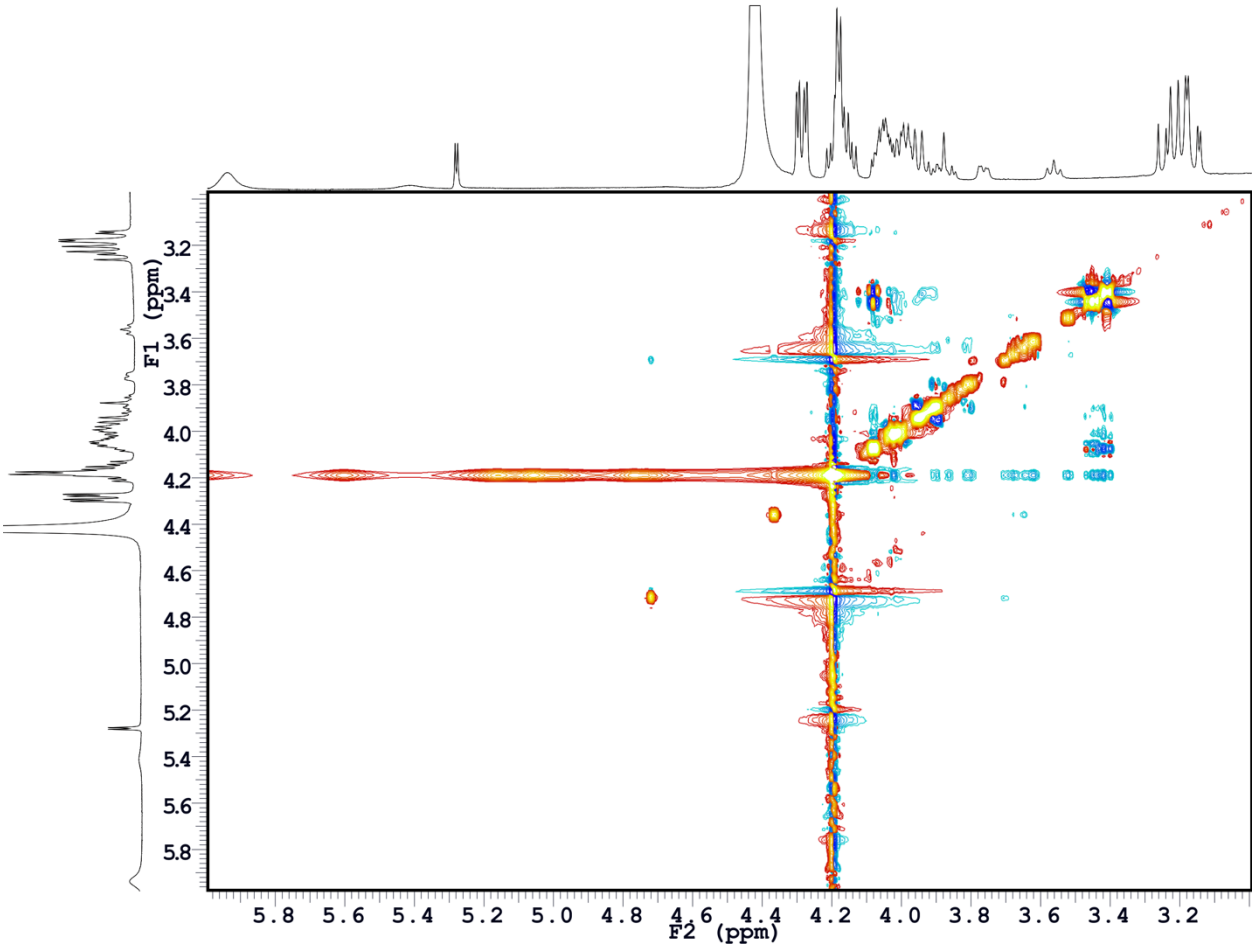

Figure S7. 2D NOESY NMR spectrum of trehalose-loaded reverse micelles, w_0=10 trehalose/water/AOT/2,2,4-trimethylpentane reverse micelles. Signals below 3 ppm arise from AOT and 2,2,4-trimethylpentane protons that do not interact with trehalose aliphatic protons. The intense signal at ~4.35 ppm arising from water leads to an artifact in the spectrum. No clear cross-peaks are observed between trehalose and AOT protons.

S2. Considerations for RM size anomalies

The most common parameter characterizing reverse micelle (RM) size is the ratio of polar solvent (usually water) to surfactant, w_0 =[polar solvent]/[surfactant]. If the amount of surfactant in a RM solution is constant, addition of water to that solution causes an increase in

the RM size with a concomitant reduction in the RM concentration.[2-3] This is well documented in the literature, which shows that RM sizes increase with increasing water to surfactant ratio, *i.e.*, w_0.[3-6] By the same argument, but not well documented, addition of surfactant to a solution containing RMs while keeping water content constant leads to a decrease in the RM size with a concomitant increase the concentration of RMs.[7] When we add AOT to a RM solution, intentionally adding surface area to existing RMs, we observe a reduction in the RM size; when we add water increasing the polar volume, the RMs get larger as predicted by $w_0 = H_2O]/[AOT]$.

We considered several effects to account for the unexpected size variations we observed when glucose, sorbitol and trehalose are encapsulated in AOT RMs, that is, dynamic light scattering measurements of RMs show that w_0 equivalent RMs appear smaller than RMs made only with water and carbohydrate-loaded RMs appear the same size as RMs made only with water. Our major explanation rests on a change in the RM eccentricity and an increase in the AOT surface area. Here we expand descriptions of possible effects to account for our observations including expanded arguments about partial molar volume, particle eccentricity, increased pressure inside RMs (Laplace pressure), dehydration, and increased AOT surface area. At the end of this section, we present a short analysis of the statistical significance of the dynamic light scattering data.

S2.1 Partial molar volume

We considered the possibility that negative partial molar volume introduced by the carbohydrate osmolytes could account for the RM sizes we observe. Negative partial molar volume leads liquid mixtures to occupy less volume than the sum of the volumes of the individual components. Negative excess partial molar volume represents the difference between

the sum of the individual volumes and the actual volume resulting from addition of the two volumes. If the water in standard water-containing RMs had significantly lower density than bulk water, it is conceivable that addition of glucose could cause the resulting interior to become more dense. However, there is no evidence of significantly lower water density inside AOT RMs. From density measurements, D'Aprano *et al.* reported that the molar volume for water inside AOT RMs was lower than that for bulk water,[8] but simulations of AOT RMs suggest higher water density near the interface, leveling off to bulk water density toward the RM core.[9-13] Although water density can increase for exotic phases at high pressure and low temperatures, for room temperature liquid we expect very small, if any, variations in water density making negative excess partial molar volume a highly improbable explanation to account for the smaller sizes we measure for w_0 equivalent RMs and the absence of size increase for carbohydrate-*loaded* RMs. Although it is possible that the thermodynamics of an RM interior differ so substantially from bulk aqueous solution as to account for our observation, this is such an unlikely result that we reject changes in partial molar volume as an explanation for our observations.

S2.2 Intramicellar pressure

We considered the possibility that high intramicellar pressure associated with the Laplace pressure of the small RM droplets containing carbohydrate osmolytes could account for the RM sizes we observe. In small droplets, the curved surface leads to increased internal pressure described by the Laplace pressure, $\Delta P = P_{internal} - P_0 = {}^{2\gamma}/_{r}$, which marks the difference in pressure due to the surface curvature. Here $P_{internal}$ is the pressure inside the droplet, P_0 is the ambient pressure, γ is the surface tension and r is the droplet radius.[14] We considered how

intramicellar pressure might account for the anomalous sizes we measure for RMs containing carbohydrate osmolytes. Without a reliable value for the surface tension of water at a planar AOT/isooctane interface, we can place an upper limit on the Laplace pressure at the isooctane/AOT/water RM interface by using the interfacial tension of the planar isooctane/water interface, γ=48±1 mN/m,[15] or the interfacial tension at a water/AOT/air surface, γ≈40 mN/m.[16] Considering w_0=10 water/AOT/isooctane RMs, our dynamic light scattering results indicate the RM hydrodynamic diameter is 4.5 nm, which includes water and AOT molecules. From small angle neutron scattering[17] and simulations,[9-13] we estimate that the AOT layer is 1.4 nm thick and the water pool radius is r_h=(4.5)/2-1.4 = 0:9 nm. This leads to a Laplace pressure of ΔP ≈ 100MPa = 1 kbar. The presence of AOT on the droplet surface against isooctane lowers the interfacial tension and thus the internal pressure. However, even a dramatic reduction of the interfacial tension by the AOT surfactant, for example if γ were 50% or 25% lower than the interfacial tension of the water/AOT/air interface (≈10-20 mN/m), the resulting Laplace pressure would remain quite large, 250-500 bar.

Because the Laplace pressure depends only on the droplet size, it is difficult to identify how increased pressure in the RMs due to extreme curvature at the RM surface could account for our observations about RM size. For carbohydrate-loaded RMs, the internal pressure should be the same regardless of whether the RM contains carbohydrate or not. Experiments measuring the impact of high pressure up to 400 MPa on glucose:water mixtures with 0.1-0.6 mass fraction (0.01-0.13 mole fraction) report increased density with increasing pressure and attribute the change to reduced water molecular volume.[18] They report only a modest 1.05 relative density increase for 0.4 mass fraction glucose in water at 20 °C under 100 MPa=1 kbar pressure. This represents only a 5% contraction in the volume, much less than needed to account for the effects

we observe. Furthermore, their measurements demonstrated larger changes for pure water than for glucose/water mixtures. Thus, increased pressure inside RMs cannot account for the observed effects.

S2.3 Reverse micelle eccentricity

To account for the carbohydrate osmolyte containing RM sizes we observe, we considered the possibility that the RM form deviates from spherical. The spherical form maximizes volume for a given surface area and is the most efficient area/volume structure. Also, as shown in Fig. 8, a sphere possesses the minimum radius for a given volume. Assuming a spherical form for a RM makes it easy to find and describe the particle size from its diffusion constant obtained from dynamic light scattering.[3, 19] Most dynamic light scattering measurements report the average radius of an RM assuming it diffuses as a spherical particle.[4-5, 13] Assuming a spherical form for water/AOT RMs, then

$$w_0 = \frac{[H_2O]}{[AOT]} = \frac{n_{H_2O}}{n_{AOT}} = \frac{{V_{RM}}/{V_{H_2O}}}{{A_{RM}}/{A_{AOT}}} = \frac{{\frac{4}{3}\pi r^3}/{V_{H_2O}}}{{4\pi r^2}/{A_{AOT}}} = \frac{r}{3}\frac{A_{AOT}}{V_{H_2O}} \quad \text{(S1)}$$

where V_{RM} is the RM volume, V_{H_2O} is the volume occupied by a water molecule, A_{RM} is the RM surface area, A_{AOT} is the area occupied by an AOT molecule on the RM surface, and r is the RM radius. This equation shows that if the RMs are spherical, w_0 is directly proportional to particle radius. Using the values given by Eskici and Axelsen for AOT RMs,[11] the volume of a water molecule inside the RM is $V_{core\ molecule}$=33 Å^3 and the surface area contribution of an AOT molecule is 59.1 Å^2,10 yields the relationship between water pool radius and w_0,

$$r = 3\frac{V_{H_2O}}{A_{AOT}}w_0 = 1.67w_0 \text{ Å} \quad \text{(S2)}$$

Equation S2 predicts a water/AOT RM with w_0 = 10 would have a water pool radius r=16.7

Å=1.67 nm, a value significantly larger than the estimate given above, $r_h = {}^{4.5}/_{2} - 1.4 = 0.9\ nm$, but of the same magnitude.

Although RMs have historically been visualized as spherical particles,[6, 17, 20] a few studies, especially recent simulations, have suggested that AOT RMs possess ellipsoidal rather than spherical forms.[9, 11-13] Eskici and Axelsen recently reported a detailed analysis of $w_0 = 7.5$ AOT RMs, comparing their results from molecular dynamics simulations to AOT RM sizes that were measured experimentally using dynamic light scattering, small angle x-ray scattering, fluorescence recovery after photobleaching, and viscosity measurements; they showed that the RMs were prolate ellipsoids. Carlstroem and Halle[21] interpreted the results from ^{2}H and ^{17}O NMR spin-relaxation studies of D_2O/AOT/isooctane RMs as due to either oblate (disc-shaped) spheroids with an aspect ratio (b/a) of 3, or to prolate (lozenge-shaped) with an aspect ratio of 0.33.

If addition of carbohydrate to the RMs causes a reduction in their eccentricity, then we expect dynamic light scattering measurements to show a reduction in the average RM size. To explore this possibility, we consider a geometric perspective. The volume of an ellipsoid is

$$V_{ellip} = \frac{4}{3}\pi abc \qquad \text{(S3)}$$

where a, b, and c are the primary, secondary, and tertiary radii of the ellipsoid, respectively. Unlike the simple analytical form for the volume of an ellipsoid, the general formula for the surface area of an ellipsoid cannot be expressed as an analytical function that describes both prolate and oblate ellipsoids. A common approximation of the ellipsoid surface area (accurate to within ±1%) is

$$A_{ellip} = 4\pi \sqrt[1.6]{\frac{(ab)^{1.6}+(ac)^{1.6}+(bc)^{1.6}}{3}} \qquad \text{(S4)}$$

When $r=a=b=c$, both expressions for the ellipsoid volume and surface area simplify to the forumlae for a sphere, $V_{sphere} = {}^{4}/_{3}\,\pi r^3$, and $A_{sphere} = 4\pi r^2$.

We simplify the situation by considering a spheroid, that is, an ellipsoid with two of the axes equal and only two characteristic radii, a and b. When $b<a$ the spheroid is prolate; when $b>a$ the particle is oblate. Figure 8 shows the deviation in particle radius, area, and volume for a spheroid of constant w_0. This figure shows that ellipsoidal particles will appear to have larger average radius compared to spherical particles. Dynamic light scattering signals arising from spherical particles should also display lower polydispersity compared to ellipsoids because diffusion is equivalent along any direction for a spherical particle. We estimate that if addition of carbohydrate causes the average RM eccentricity to change from (b/a)= 2.5 to 2.0 (prolate) or 0.63 to 0.56 (oblate) we would observe a 10% reduction in size. We believe that a reduction in eccentricity presents a reasonable mechanism to explain our observations.

2.4 Dehydration or mass loss to continuous phase

We considered the possibility that addition of carbohydrate osmolyte to the RMs leads to a dehydration-like event where carbohydrates recruit water out of the RMs. The possibility of dehydration is most easily explained with an example: consider a glucose-loaded w_0 = 10 AOT RM. Assuming that ~1000 water and ~100 AOT molecules normally comprise a w_0=10 RM,[11, 22] then using the values given by Eskici and Axelsen for AOT (r_{AOT}=13.9 Å, A_{AOT}=59.1 Å^2, $V_{core\ molecule}$=33 Å^3) loading the w_0=10 RM with one glucose per 30 water molecules, adds ~33 glucose molecules to each RM. Estimating the glucose molecular volume, $V_{glucose}$=187.04 Å^3/molecule from the solid density[23] and molar mass, each glucose molecule has approximately the same volume as 5.7 water molecules. If all 33 glucose molecules reside in the volume of the RM, then

we should see a ~23% increase in the RM size. Simplistically, if none of the glucose molecules were solubilized inside the RMs, the RM would remain the same size. However, glucose is completely insoluble in alkane solvents and our NMR results demonstrate significant interaction between water and glucose and no interaction between AOT headgroup protons with glucose protons. Additionally, when glucose is not absorbed by the RMs, we observe solid glucose in the sample vial. Thus, we feel confident that all the glucose is in the RM water pools.

Another possibility would be if each RM shed a water volume equivalent to the added glucose volume then the initial RM size would be maintained. However, this would require more than 20% of the water in the sample to exist outside the RMs. This amount of water would easily be visible to the naked eye and observable in our hexane-d_{14} NOESY spectrum. The insolubility of glucose or water in isooctane makes any such scenario unphysical. Our attempts to dissolve dry or hydrated carbohydrates directly in isooctane in the absence of AOT resulted in precipitation and/or phase separation; no particles were observed either as a turbid solution or via dynamic light scattering. Because they would remove surfactant from contributing to RM surface area, any aggregates comprising only surfactant and carbohydrate should yield larger w_0 hence larger, not smaller, particles. Thus, dehydration cannot account for our dynamic light scattering RM size observations.

S2.5 AOT headgroup area increase

We considered the possibility that addition of carbohydrate osmolyte to the RMs leads the AOT surfactants to occupy more area, that is, to expand the surface area per surfactant molecule. As described in the manuscript, this situation has been observed for lipid bilayers in the presence of carbohydrate osmolytes.[24] Here we present the geometric argument

demonstrating how much expansion would be required.

We can estimate the area of the AOT molecule beginning with the relationship between w_0 and particle radius $w_0 {}^{V_{H_2O}}\!/_{A_{AOT}} = {}^{r}\!/_{3}$, equation S1. Rearranging this equation yields $A_{AOT} = 3w_0 {}^{V_{H_2O}}\!/_{r}$; however to use this expression requires estimation of the difference between hydrodynamic radius and water pool radius. If, instead, we assume the surfactant tail layer is constant between RMs we can use a difference equation:

$$w_0\left(\frac{V_{H_2O}}{A_{AOT}} - \frac{V_{H_2O}}{A_2}\right) = \frac{r_1 - r_2}{3} \qquad \text{(S5)}$$

Using A_{AOT}=33 Å^2, V_{H_2O}=30 Å^3,[11] and $r_1 - r_2 = 10$ Å for w_0 =10 and 38 Å for w_0=40, gives a headgroup area of A_2 = 53 Å^2 and 50 Å^2, respectively. This represents an increase in the average distance between AOT headgroups of approximately 26% for w_0 =10 and 23% for w_0 = 40 RMs. Although this is a fairly large increase, it is not outside the realm of plausibility, and is the upper limit for the size increase. The actual headgroup size increase is likely smaller than these values, as some RM radius decrease is due to the other effects on particle size (*i.e.*, eccentricity) we have also discussed.

S2.6 Statistical considerations

Examining Fig. S8 it is easy to see that the average diameter of both standard and w_0 *equivalent* RMs containing glucose have different average diameters, but as the particle size distribution (PSD) of each overlaps, it is not clear that the difference in size between the two sets of particles is *statistically significant*, simply through observation. This can be more clearly demonstrated by combining the two distributions together, as the gold lines in Fig. S8. From these graphs, it is clear that the w_0=40 RM solutions have distinct sizes even when the data is

combined, while the w_0=10 solutions simply present a single average size with a broader polydispersity. To be confident that the w_0=10 RMs represent different RM sizes, we performed a Student's t-test comparing the average diameters of the standard RM solutions to those of the w_0 equivalent RM solutions. The null hypothesis of this t-test is $H_0 : \bar{d}_{RM} - \bar{d}_{eq} = 0$ or that there is no statistical difference between the average diameter of the standard RMs and the w_0 equivalent RMs. The result of this test shows that we reject the null hypothesis with extreme prejudice ($p = 1.3 \times 10^{-19}$). Thus we are confident that the standard water-containing and w_0 equivalent RMs are different sizes.

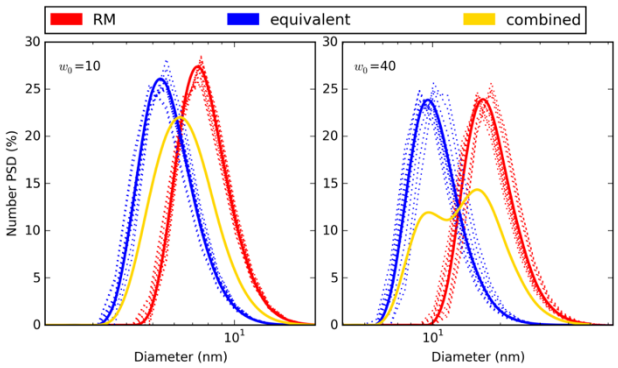

Figure S8: The particle size distribution (PSD) of both standard (**red** dots) and w_0 equivalent (**blue** dots) RMs. Averaging the standard and w_0 equivalent PSDs separately gives two distinct average PSDs (solid **red** and **blue** lines) and combining the two (**gold** lines) yields a single distribution for w_0=10 and a bimodal one for w_0=40

References

1. Keeler, J., *Understanding NMR Spectroscopy*. John Wiley & Sons: New York, 2011.

2. Frense, D.; Haftendorn, R.; Ulbrich-Hofmann, R., 2-Modified 1,3-Diacylglycerols as New Surfactants for the Formation of Reverse Micelles. *Chem. Phys. Lipids* **1995,** *78*, 81-87.

3. Bohidar, H. B.; Behboudnia, M., Characterization of Reverse Micelles by Dynamic Light Scattering. *Colloid Surf. A* **2001,** *178*, 313-323.

4. El Aferni, A.; Guettari, M.; Tajouri, T., Determination of the Water/AOT/Isooctane Reverse Micelles Size Parameters from Their Refractive Index Data. *J. Solut. Chem.* **2017,** *46*, 89-102.

5. Khan, M. F.; Singh, M. K.; Sen, S., Measuring Size, Size Distribution, and Polydispersity of Water-in-Oil Microemulsion Droplets Using Fluorescence Correlation Spectroscopy: Comparison to Dynamic Light Scattering. *J. Phys. Chem. B* **2016,** *120*, 1008-1020.

6. Zulauf, M.; Eicke, H. F., Inverted Micelles and Microemulsions in the Ternary System Water/Aerosol-OT/Isooctane as Studied by Photon Correlation Spectroscopy. *J. Phys. Chem.* **1979,** *83*, 480-486.

7. Odella, E.; Falcone, R. D.; Silber, J. J.; Correa, N. M., How Topo Affects the Interface of the Novel Mixed Water/AOT:TOPO/N-Heptane Reverse Micelles: Dynamic Light Scattering and Fourier Transform Infrared Spectroscopy Studies. *Phys. Chem. Chem. Phys.* **2014,** *16*, 15457-15468.

8. D'Aprano, A.; Donato, I. D.; Goffredi, M.; Liveri, V. T., Volumetric and Transport-Properties of Aerosol-OT Reversed Micelles Containing Light and Heavy-Water. *J. Solut. Chem.* **1992,** *21*, 323-332.

9. Abel, S.; Sterpone, F.; Bandyopadhyay, S.; Marchi, M., Molecular Modeling and Simulations of AOT-Water Reverse Micelles in Isooctane: Structural and Dynamic Properties. *J. Phys. Chem. B* **2004,** *108*, 19458-19466.

10. Chowdhary, J.; Ladanyi, B. M., Molecular Dynamics Simulation of Aerosol-OT Reverse Micelles. *J. Phys. Chem. B* **2009,** *113*, 15029-15039.

11. Eskici, G.; Axelsen, P. H., The Size of AOT Reverse Micelles. *J. Phys. Chem. B* **2016,** *120*, 11337-11347.

12. Martinez, A. V.; Dominguez, L.; Malolepsza, E.; Moser, A.; Ziegler, Z.; Straub, J. E., Probing the Structure and Dynamics of Confined Water in AOT Reverse Micelles. *J. Phys. Chem. B* **2013,** *117*, 7345-7351.

13. Vasquez, V. R.; Williams, B. C.; Graeve, O. A., Stability and Comparative Analysis of AOT/Water/Isooctane Reverse Micelle System Using Dynamic Light Scattering and Molecular Dynamics. *J. Phys. Chem. B* **2011,** *115*, 2979-2987.

14. Thiam, A. R.; Farese, R. V., Jr.; Walther, T. C., The Biophysics and Cell Biology of Lipid Droplets. *Nat. Rev. Mol. Cell Biol.* **2013,** *14*, 775-786.

15. Spildo, K.; Blokhus, A. M.; Andersson, A., Surface and Interfacial Properties of Octanoic Acid–Octylamine Mixtures in Isooctane–Water Systems: Influence of Acid: Amine Molar Ratio and Aqueous Phase Ph. *J. Colloid Interface Sci.* **2001,** *243*, 483-490.

16. Datwani, S. S.; Stebe, K. J., Surface Tension of an Anionic Surfactant: Equilibrium, Dynamics, and Analysis for Aerosol-OT. *Langmuir* **2001,** *17*, 4287-4296.

17. Kotlarchyk, M.; Huang, J. S.; Chen, S. H., Structure of AOT-Reversed Micelles Determined by Small-Angle Neutron-Scattering. *J. Phys. Chem.* **1985,** *89*, 4382-4386.

18. Werner, M.; Baars, A.; Werner, F.; Eder, C.; Delgado, A., Thermal Conductivity of Aqueous Sugar Solutions under High Pressure. *Int. J. Thermophys.* **2007,** *28*, 1161-1180.

19. Tovstun, S. A.; Razumov, V. F., What Makes AOT Reverse Micelles Spherical? *Colloid Polym. Sci.* **2015,** *293*, 165-176.

20. De, T. K.; Maitra, A., Solution Behaviour of Aerosol OT in Non-Polar Solvents. *Adv. Coll. Interface Sci.* **1995,** *59*, 95-193.

21. Carlstroem, G.; Halle, B., Shape Fluctuations and Water Diffusion in Microemulsion Droplets: A Nuclear Spin Relaxation Study. *J. Phys. Chem.* **1989,** *93*, 3287-3299.

22. Piletic, I. R.; Moilanen, D. E.; Spry, D. B.; Levinger, N. E.; Fayer, M. D., Testing the Core/Shell Model of Nanoconfined Water in Reverse Micelles Using Linear and Nonlinear IR Spectroscopy. *J. Phys. Chem. A* **2006,** *110*, 4985-4999.

23. National Center for Biotechnology Information. Pubchem Compound Database; Cid=5793, Source: Ilo-Icsc, https://pubchem.ncbi.nlm.nih.gov/compound/5793 (accessed June 29, 2017).

24. Andersen, H. D.; Wang, C.; Arleth, L.; Peters, G. H.; Westh, P., Reconciliation of Opposing Views on Membrane-Sugar Interactions. *Proc. Natl. Acad. Sci. U. S. A.* **2011,** *108*, 1874-1878.